Towards a Hardware Implementation of Ultra–Wideband Beamforming

Philipp K. Gentner[1], Wolfgang Gartner[1], Geoff Hilton[2], Mark E. Beach[2], Christoph F. Mecklenbräuker[1,3]

[1] *Institute of Communications and Radio-Frequency Engineering, Vienna University of Technology*
Gusshausstrasse 25/389, 1040 Wien, Austria
[2] *Centre for Communications Research, University of Bristol*
Merchant Venturers Building, Woodland Road,Bristol,United Kingdom
[3] *Christian Doppler Laboratory for Wireless technologies*
for sustainable mobility
philipp.gentner@nt.tuwien.ac.at

***Abstract*—This paper discusses and analyses the hardware implementation of an ultra-wideband (UWB) beamformer for UWB Impulse Radio data transmission. We use a Complex Programmable Logic Device (CPLD) acting as the binary baseband information source. The CPLD provides input to a pulse shaper and subsequently to a four-element array of UWB antennas. This smart antenna system comprises the digital baseband part, the radio-frequency frontend, and the antenna array. For this contribution, we discuss the design, implementation, and UWB measurement results obtained in an anechoic chamber.**

I. Introduction

We design a four-element UWB smart antenna to enable beamforming and –steering for UWB impulse radio applications. This topic has raised increased interest ([1] and [2]) for future wireless networks in indoor environments and for short-range, power-efficient connectivity at medium to high data rates. The potential applications are manifold, e.g. to send high-definition audio-visual content to displays and loadspeakers. Broadband planar horn antennas are not suitable as array elements, because they cannot be embedded into display screens and gaming consoles. We focus only on small planar, wideband monopole antennas.

The high time-bandwidth product of UWB transmissions enables estimating the distances between nodes. Subsequently, location-aware coding can stabilize/enhance the achievable data rate and mitigate interference to/from legacy networks.

In this work, four small planar printed monopoles with a rectangular shape [3] and four elliptical slot monopoles [4] are manufactured and individually driven by a pulser prototype printed circuit board (PCB). This paper is organised as follows: In section II, antenna measurements in the far– and near-field are documented and discussed which were taken in the anechoic chamber of Bristol University. We show that in both the near– and the far-field scenarios, beamforming in a specific frequency band is feasible. In the section III, we present the hardware platform which allows to drive each single antenna element. Finally, in section IV, the first time domain measurements in an office scenario of the platform with an UWB antenna array are discussed and analysed.

II. Antennas

This section is divided into two parts, i.e. the far-field and the near-field measurement parts, in which we present frequency domain measurements performed in an anechoic chamber. It is well known that for wideband antennas as single elements and their arrangement in an array, the main lobe is not stable because it tends to change the steering direction versus frequency. To avoid effects of cable currents and reflections from the rotational fixture, the elements are put on a rectangular metal plate with a size of $360 \times 270\,\mathrm{mm}^2$. To drive the four wideband antennas in an array a 1-to-4 Wilkinson splitter is used, which is mounted behind the metal plate.

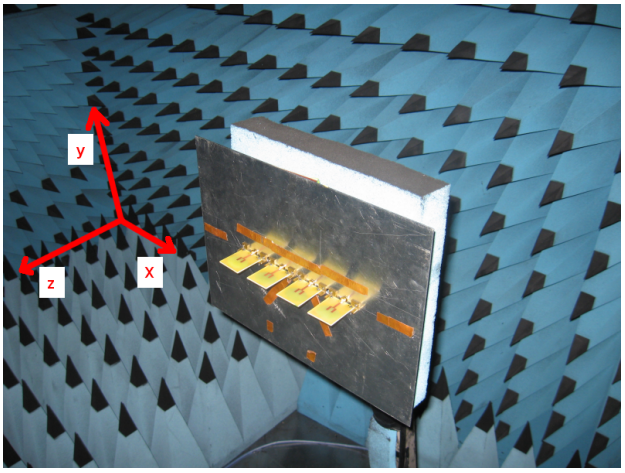

Fig. 1. Photo of elliptical monopole array inside the anechoic chamber. The figure shows the coordinate system used for all radiation pattern measurements.

A. Farfield Measurements

To investigate the effect of beam stability in the farfield, the following procedure is carried out for two different antenna types:

1) Full 3D pattern measurement for the single element at selected frequencies.

2) Full 3D pattern measurement for the array $d_i = 5\,\text{cm}$ and $d_i = 10\,\text{cm}$ at selected frequencies.
3) H-plane / E-plane frequency-resolved measurement.

The first two steps allow us to evaluate the directivity of the single element and four-element array at spot frequencies. Although this is insufficient to fully interpolate results for wideband performance, it does give specific directivity markers for the wideband measurements. It should be noted that in any characterisation of the antenna under test, the frequency-dependent gain of the other antenna in the link and the frequency-dependent losses of cables add uncertainty in to the wideband measurements - hence the need for these single point measurement to normalise the data.
In the third step, the wideband array behaviour can be analyzed in the frequency domain versus an angular dimension, which enables the transformation to the time domain [5].

Table I shows a summary of the captured measurements for 3-10GHz.

Figures 2, 3 and 4 show the results of 3D pattern measurements of a single elliptical monopole at different frequencies. The figures show the relative gain on the left side and an azimuthal polar plot at $\phi = -90°$ on the right side. While at 3GHz (Figure 2) the radiation pattern is almost omnidirectional in the half sphere, the radiation pattern shows a deep notch at $\theta = -60°$ and $\theta = 60°$ at a measurement frequency of 5 GHz. At 7 GHz, we note that the antenna becomes more directional towards $\theta = -90°$ and $\theta = 90°$. With the change in pattern shape, the (maximum) directivity of the element is 5,32dB at 3GHz, 8.33dB at 5 GHz and increasing to 5.26dB at 7GHz.

In Step 2, the elliptical monopoles are used as elements in a linear four-element array (Fig.1). All four elements are identical in design and the inter-element spacing is 5 cm. The results presented in Figs. 5, 6, and 7, are measured at the same set of frequencies as before.

As expected the azimuth beam narrows due to the beamforming effect. The elevation beam shows the same characteristic of the main beam as the single element. The lobes remain at nearly constant elevation angles, however, the notch becomes less deep (see $\theta = -60°$ and $\theta = +60°$).

The frequency resolved measurements are taken for each individual angular step of the turntable. To calculate the gain of the wideband antenna, a calibration measurement is performed (Fig. 8). A second reference antenna of identical type (Flann DP240) is used and positioned on the rotational fixture in the anechoic chamber.

The gain of the antenna under test is given by Eq.(4)

$$s_{21DUT} = L_1 + L_2 + G_2 + G_1 \quad (1)$$

$$s_{21REF} = L_1 + L_2 + G_1 + G_1 \quad (2)$$

$$s_{21} = s_{21DUT} - s_{REF} = G_2 - G_1 \quad (3)$$

$$G_2 = s_{21DUT} - s_{REF} + G_1 \quad (4)$$

The gain is calculated in a post processing step for the single antenna element and the four element array. Figure 9 shows a frequency resolved gain versus azimuth ϕ (x-z plane). The

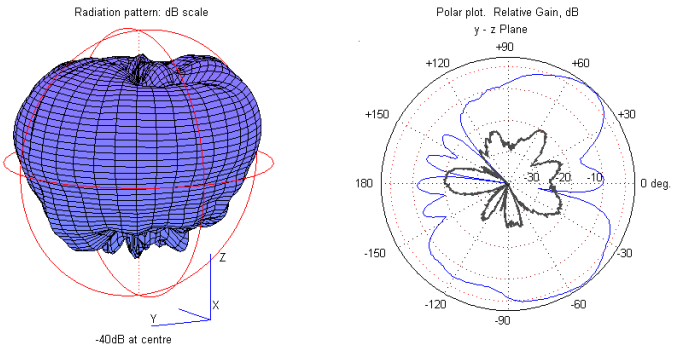

Fig. 2. Co Polarisation Full Pattern - Single Elliptical Monopole at 3000 MHz.

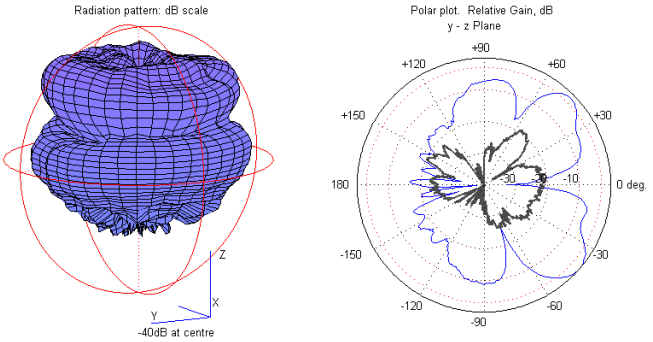

Fig. 3. Co Polarisation Full Pattern - Single Elliptical Monopole at 5000 MHz.

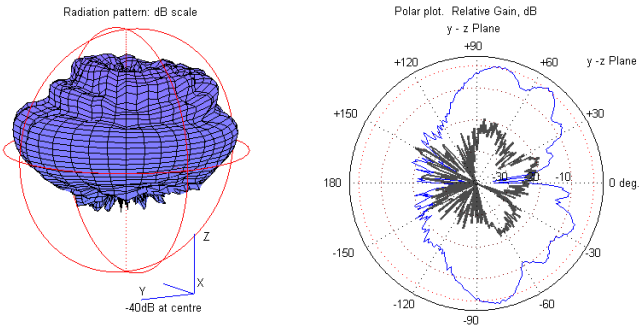

Fig. 4. Co Polarisation Full Pattern - Single Elliptical Monopole at 7000 MHz.

transmission coefficient s_{21} is measured in the farfield at a distance of 5.4 m in the same manner as for the single element. The strong main lobes, which are visible along the azimuth direction at $\phi = \pm 90°$ are at the front and back sides of the array (Fig.11). The frequency behaviour of the main lobes can be summarized as follows: The beamwidth of the main lobes decreases for increasing frequency and the first sidelobes shift towards the main lobe. A new sidelobe appears around 4 GHz. The metal plate shifts the main beam in the y - z plane as one can see in Figs. 5,6 and 7. The frequency resolved measurement with the result in Fig. 11 is captured with an offset of 45° to be able to analyze the main lobe.

	Farfield d = 5,4m						Nearfield (Array d_i = 5cm)					
Antenna	Single		Array d_i=5cm		Array d_i=10cm		d = 1m		d = 0.85m		d = 0.66m	
	3D pattern	Plane	3D pattern	Plane	3D pattern	Plane	3D pattern	Plane	3D pattern	Plane	3D pattern	Plane
ellipt	3 GHz	1	3 GHz	1	3 GHz	1						
	5 GHz	2	5 GHz	3	5 GHz	2						
	7 GHz		7 GHz		7 GHz	3						
	8,5 GHz		8,5 GHz		8,5 GHz							
	10 GHz		10 GHz		10 GHz							
	3D pattern	Plane	3D pattern	Plane	3D pattern	Plane	3D pattern	Plane	3D pattern	Plane	3D pattern	Plane
rect	3 GHz	1	3 GHz	1	3 GHz		3 GHz	1	3 GHz		3 GHz	1
	5 GHz	2	5 GHz	2	5 GHz		5 GHz	2	5 GHz	2	5 GHz	2
	7 GHz		7 GHz		7 GHz		7 GHz		7 GHz		7 GHz	
	8,5 GHz											
	10 GHz											

TABLE I
MEASUREMENTS TAKEN IN THE ANECHOIC CHAMBER. (PLANE 1 IS THETA -90:5:90, PHI = 0DEG),(PLANE 2 IS THETA 90DEG, PHI = -90:5:90),(PLANE 3 IS THETA 45DEG, PHI = -90:5:90)

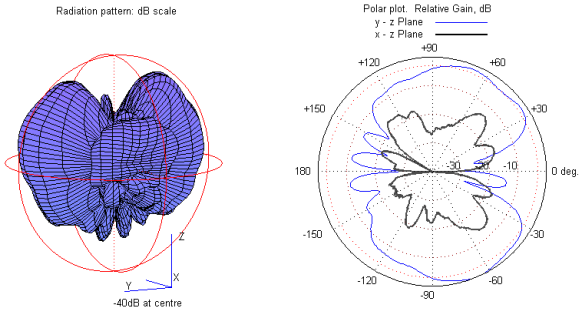

Fig. 5. Co Polarisation Full Pattern - Elliptical Monopole Array at 3000 MHz

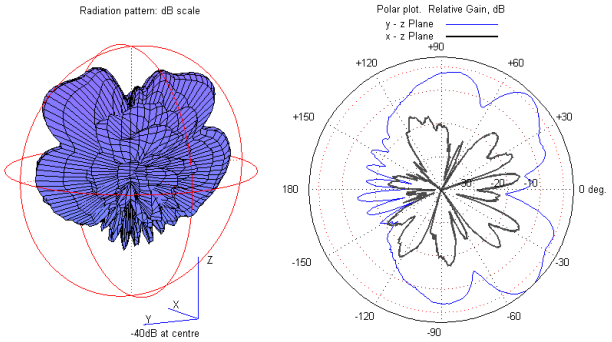

Fig. 6. Co Polarisation Full Pattern - Elliptical Monopole Array at 5000 MHz

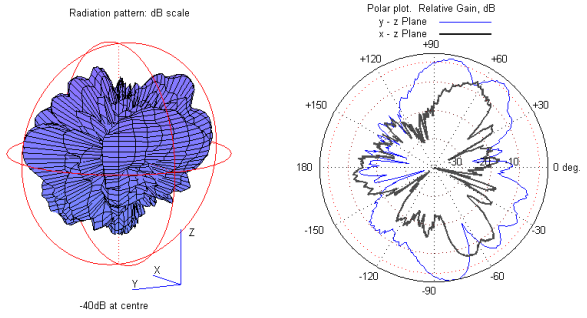

Fig. 7. Co Polarisation Full Pattern - Elliptical Monopole Array at 7000 MHz

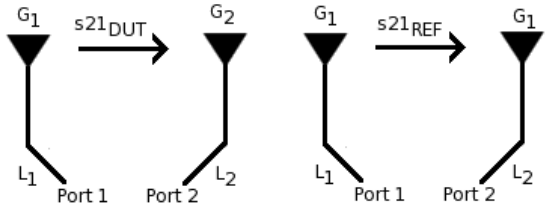

Fig. 8. Calibration calculation process for two antennas connected to the a two port vector network analyzer.

The main lobe has an average gain of 10 dB across a bandwidth of 3.5 GHz.

B. Near field measurements

The achievable datarate for UWB transmission in the nearfield can be extremely high. For this reason, nearfield measurements are carried out (Fig. 15). In the nearfield of the antenna array, full 3D pattern measurements are carried out at distances $d = 1$ m, $d = 0.85$ m, and $d = 0.66$ m from the reference horn to the antenna under test. The antenna under test for this investigation is the rectangularly shaped monopole. In Figs. 12, 13, and 14 we observe that the main beam has almost constant width versus distance. Here the data is presented in terms of the transmission coefficient (S_{21}) since antenna gain figures are not really valid at these distances. A missing data point is visible as a non constant curve in all 0.66m distance transmission coefficient graph.

III. HARDWARE DESCRIPTION

A commercially available evaluation kit with a Complex Programmable Logic Device (CPLD [6]) is used to generate a rectangular signal. The rising edge of the rectangular signal is used to create a pulse. The frequency of the rectangular signal and therefore the pulse repetition frequency can be adjusted by changing the crystal oscillator of the board. At the moment a 20 MHz clock oscillator is used, which ends in 10 MHz pulse repetition frequency. Random pulse sequence and continuous pulse sequence can be set, as well as a single antenna element

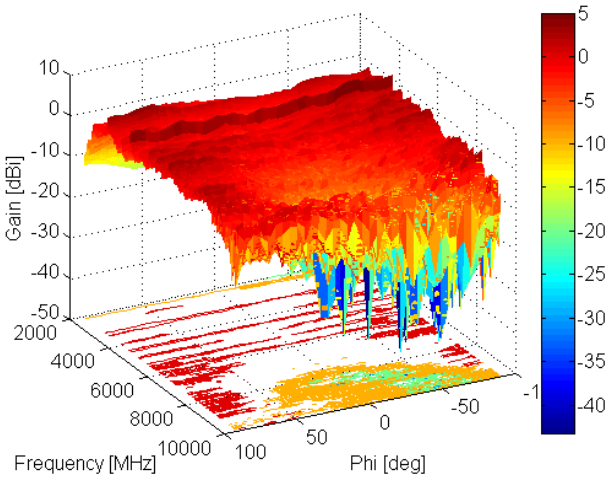

Fig. 9. Single elliptical monopol antenna

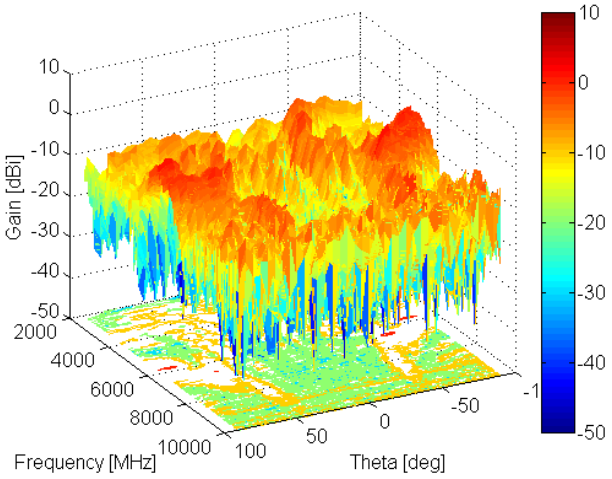

Fig. 10. Elliptical monopol array with 4 elements E-plane

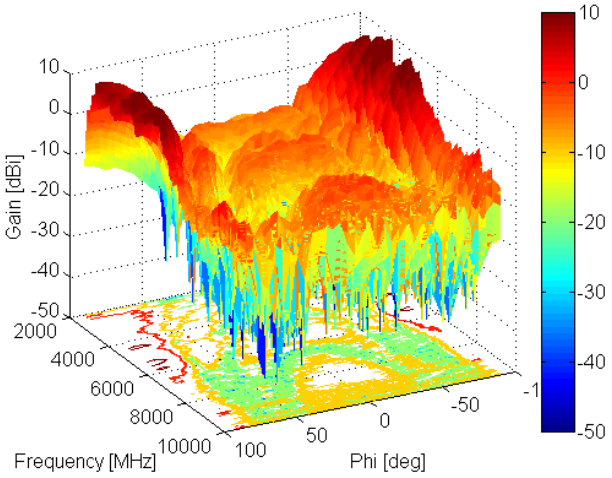

Fig. 11. Elliptical monopol array with 4 elements H-plane + Theta 45 deg.

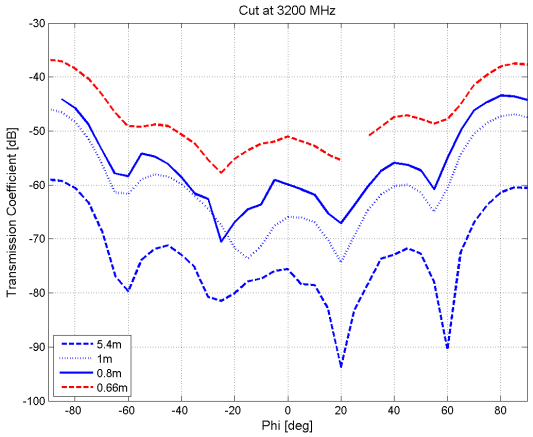

Fig. 12. Near - Farfield Comparison at 3200 MHz.

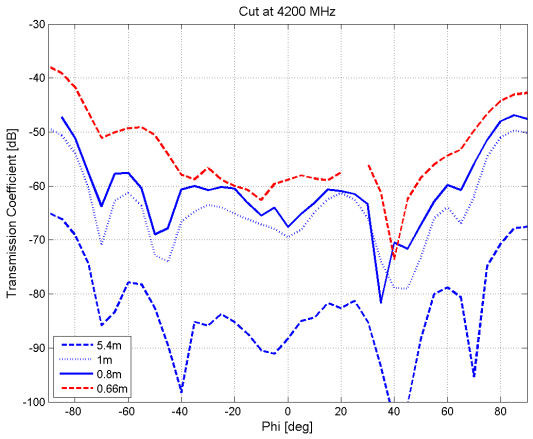

Fig. 13. Near - Farfield Comparison at 4200 MHz.

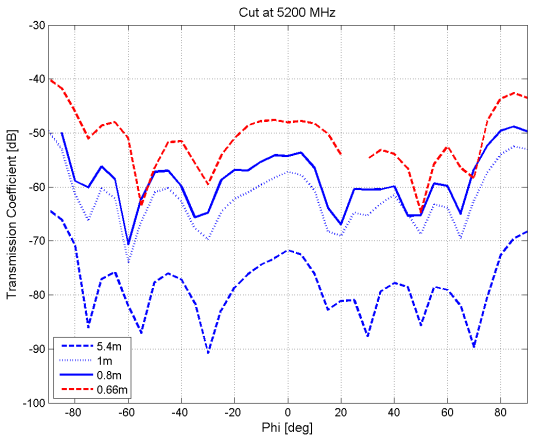

Fig. 14. Near - Farfield Comparison at 5200 MHz.

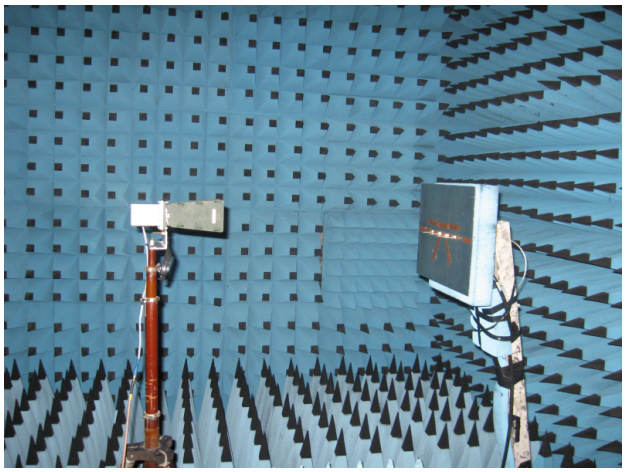

Fig. 15. Nearfield measurement Setup.

for calibration purpose can be selected. To switch through the 4 antennas a state machine, programmed in VHDL, is used. Inside the state machine the sequential characteristic of the IF-function is used to give buttons and two switches a priority.

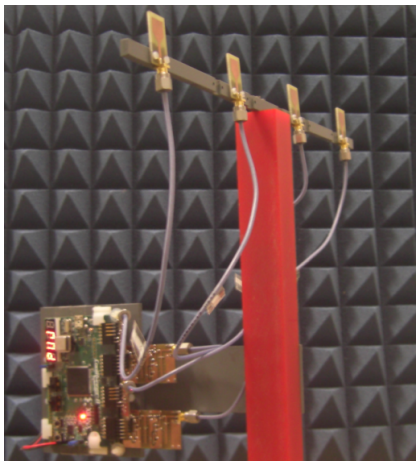

Fig. 16. Linear array with four broadband antenna elements on a rotational setup. The Complex Programmable Logic Device acts as data source and control unit.

The pulse shaper design [7] was manufactured and showed by measurement a pulsewidth of 360 ps with a peak-to-peak voltage of 1.75V with less ringing (Fig. 18). Two repetitive stages consisting of a highpass, a npn-transistor and a shorted stub line make the pulse shaper (Fig. 17). Measurements also show, that the pulse shape does not change if the pulse repetition frequency is increased.

The measurement setup exists of a rotatable fixture, where the hardware is mounted on (Fig. 16). The antenna elements are placed in a linear formation on top and are connected to the pulsers. The rectangularly shaped monopoles [3] are used as antenna under test for this investigation. The interelement distance can be changed easily for analysis of grating lobes.

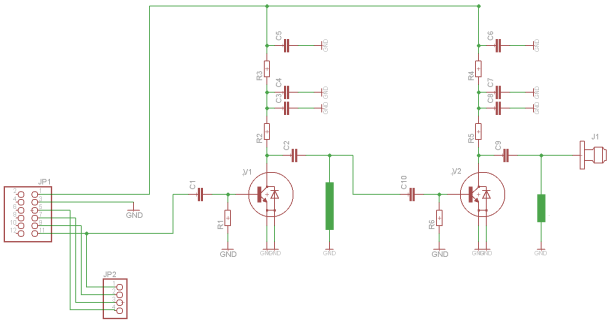

Fig. 17. Schematic of the pulse shaper [7].

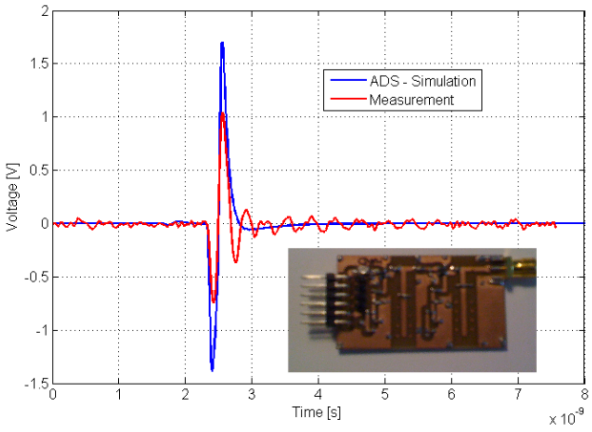

Fig. 18. Simulated and measured output of the pulse shaper.

IV. Time Domain Measurements

In this section, time domain measurements are made in an office scenario with UWB antennas. A broadband horn antenna acts as the reference antenna and is placed for the first measurements about 60cm apart from the array. Between the array under test and the reference antenna an absorber was placed, to avoid any reflecting waves from the table. We present these first measurements in time domain versus azimuth angle for an interelement distance of 5cm (Fig. 19). For the measured array we see a tilt of the main pulse beam of about 12 degrees in azimuth. This can be explained that the pulser connected to the antenna, which has the longest distance towards the reference antenna, has less gain than the other pulsers. Appearance of unwished pulse maximas besides the main lobe can be seen in the time domain measurement of an UWB array if the element distance increases.

The logic device is connected with a trigger signal to the digital sampling oscilloscope. So we can observe the pulse appearance from the array to the reference antenna in time. In Fig. 20 and Fig. 21 one can see the pre oscillation of the pulse, which has the maximum distance in time and space at the 0 degree azimuth line. Again in endfire direction at -90 degree the weak pulser element can be seen.

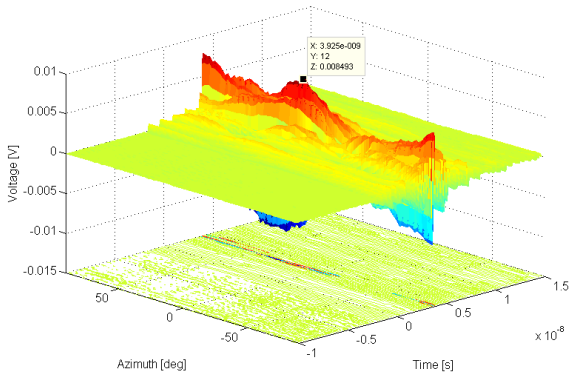

Fig. 19. Azimuth versus time of the measured pulse, in a distance of 60cm with a interelement distance of 5 cm.

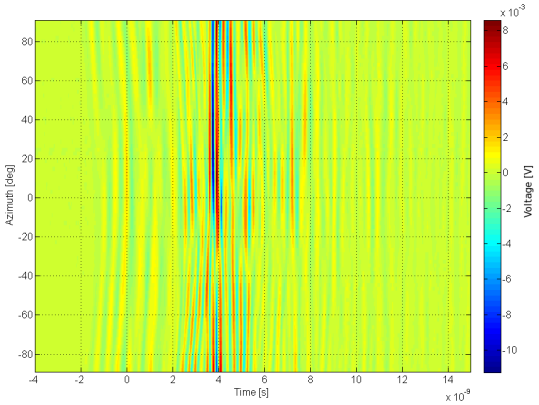

Fig. 20. Two dimension plot of azimuth versus time for a linear antenna array with 5cm distance of the elements.

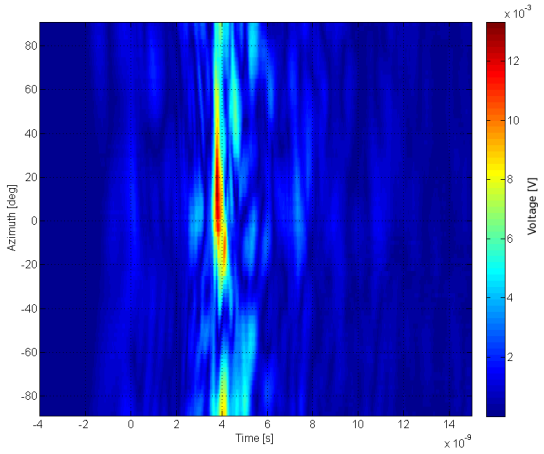

Fig. 21. Envelope of the measured time domain pulse calculated from the corresponding analytic signal.

V. CONCLUSIONS

This paper has considered the element performance, array performance and system performance of a 4-element ultra-wideband system capable of beamsteering and based upon Impulse Radio. It has been shown that the shape of the co-polar radiation pattern and directivity alter considerably with frequency (a directivity variation of 3dB for spot frequencies between 3-7GHz). Wideband measurements (3-10GHz for the azimuth plane) indicate that the main lobe maintains an average gain of 10dB across a 3.5GHz bandwidth. Furthermore, since we are interested in ultrawideband transmission over short distance (less than 1m), near field measurements were undertaken that indicate that the width of the main beam does not alter to any considerable amount with distance. The final part of the paper looked at the time domain performance of the array in an office. With this near field time resolved measurement, it is shown that the short pulse adds constructive in the main beam. This concludes that it is possible to use the small UWB antennas for beam steering in a certain frequency range. For further investigations the pulsers will be upgraded to become adjustable active delay lines [1].

VI. ACKNOWLEDGMENT

This work is partly supported by the Christian Doppler Laboratory for Wireless Technologies for Sustainable Mobility. The authors would like to thank for the member's support during manufacturing and measurements. The authors would also like to thank COST 2100 for funding the measurement campaign UWBeams (Ultra WideBand Beamforming and Beamsteering to enhance the datarate for mobile devices) at Bristol University, as a Short Term Scientific Mission.

REFERENCES

[1] H. Hashemi, T. Chu, and J. Roderick; *"Integrated True-Time-Delay-Based Ultra-Wideband Array Processing"*,2008, IEEE Communications Magazine, September 2008, pp. 162 - 172

[2] S. Ries, and T.Kaiser: *"Highlights of UWB impulse beamforming"*, Proceedings EUSIPCO 2004, Vienna 2004

[3] J. Jung, W. Choi and J. Choi, P. Miskovsky, C. Ibars, J. Mateu, M. Navarro; *"A small Wideband Microstrip-fed Monopol Antenna"*, 2005, Microwave and Wireless components Lett., Vol. 15, No. 10, pp. 703-705

[4] P. Li, J. Liang and X. Chen: *"Ultrawideband printed elliptical slot antenna fed by tapered microstrip line with Ushaped tuning stub"*, Microwave Opt. Technol. Lett., Vol. 47, No. 2, pp. 140143, 2005

[5] W. Soergel, C. Sturm, W. Wiesbeck; *"Impulse Responses of Linear UWB Antenna Arrays and the Application to Beam Steering"*, 2005, International Conference on Ultra-Wideband, September 2005, pp. 275 -280

[6] http://www.xilinx.com/products/coolrunner2/index.htm

[7] M. G. Di Benedetto, T. Kaiser, A. F. Molisch, I. Oppermann, C. Politano, and Domenico Porcino: *"UWB Communication Systems: A Comprehensive Overview"*, Eurasip Signal Processing and Communications, ISBN 9775945100, 2006